

pubs.acs.org/JACS Article

# Efficient Modeling of Organic Chromophores for Entangled Two-Photon Absorption

Gyeongwon Kang, Kobra Nasiri Avanaki, Martín A. Mosquera, Ryan K. Burdick, Juan P. Villabona-Monsalve, Theodore Goodson, III, and George C. Schatz\*



Cite This: J. Am. Chem. Soc. 2020, 142, 10446-10458



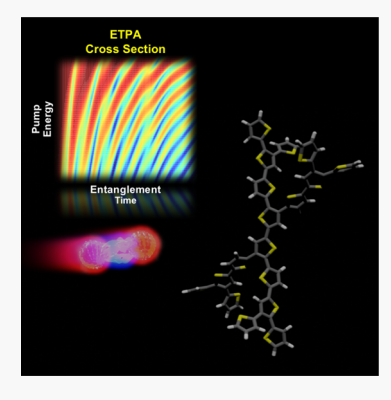
**ACCESS** 

Metrics & More

Article Recommendations

SI Supporting Information

ABSTRACT: The use of a nonclassical light source for studying molecular electronic structure has been of great interest in many applications. Here we report a theoretical study of entangled two-photon absorption (ETPA) in organic chromophores, and we provide new insight into the quantitative relation between ETPA and the corresponding unentangled TPA based on the significantly different line widths associated with entangled and unentangled processes. A sumover-states approach is used to obtain classical TPA and ETPA cross sections and to explore the contribution of each electronic state to the ETPA process. The transition moments and energies needed for this calculation were obtained from a second linear-response (SLR) TDDFT method [J. Chem. Phys., 2016, 144, 204105], which enables the treatment of relatively large polythiophene dendrimers that serve as two-photon absorbers. In addition, the SLR calculations provide estimates of the excited state radiative line width, which we relate to the entangled two-photon density of states using a quantum electrodynamic analysis. This analysis shows that for the dendrimers being studied, the line width for ETPA is orders of magnitude



narrower than for TPA, corresponding to highly entangled photons with a large Schmidt number. The calculated cross sections are in good agreement with the experimentally reported values. We also carried out a state-resolved analysis to unveil pathways for the ETPA process, and these demonstrate significant interference behavior. We emphasize that the use of entangled photons in TPA process plays a critical role in probing the detailed electronic structure of a molecule by probing light-matter interference nature in the quantum limit.

## ■ INTRODUCTION

Since the initial discovery of two-photon absorption (TPA) in the 1930s, TPA has attracted significant interest in studying fundamental aspects of light—matter interaction. In addition, the use of two-photon sources has been considered in a variety of applications including photopolymerization, optical data storage, simicrofabrication, sinch and light harvesting. With classical light sources, TPA is a second-order nonlinear optical process (Rate =  $\delta_r \phi^2$ , where  $\delta_r$  is the cross section and  $\phi$  is the photon flux), thus a very high  $\phi$  ( $\sim 10^{22}$  photons cm<sup>-2</sup> s<sup>-1</sup>) is required to overcome the small TPA cross sections. Typical cross sections for TPA in most organic chromophores are on the order of  $10^{-48}$  cm<sup>4</sup> s photon<sup>-1</sup>, and are usually quoted in the units of Goeppert-Mayer (GM), where 1 GM is  $10^{-50}$  cm<sup>4</sup> s photon<sup>-1</sup>.

Important technical developments in the past decades have occurred to facilitate TPA for the purpose of demonstrating quantum optical effects. Specifically, recent advances in nonclassical light sources of entangled photons have enabled new directions in nonlinear spectroscopy for investigating quantum effects in light–matter interaction and developing optical quantum computers. The first discovery of entangled photons was reported by Kocher and Commins in 1967, where polarization correlation of two photons

simultaneously emitted in the atomic cascade in calcium was observed. Since then, thorough studies of the properties of entangled photons have been carried out both experimentally and theoretically. Further improvements in photon detection instruments in the past decades have enabled the application of entangled photons to broader problems including entangled two-photon absorption (ETPA) spectroscopy applied to molecules. Indeed, the unique nonclassical spectral and temporal features of entangled photons make them a potentially powerful probe of molecular electronic structure.

In many ETPA experiments, entangled photons are generated through a nonlinear process called spontaneous parametric down conversion (SPDC). In SPDC, one photon of higher energy from a pump laser is converted into a pair of photons (namely, signal and idler photons) of lower energy through interaction with a nonlinear crystal. Both energy and

Received: March 11, 2020 Published: May 13, 2020





momentum are conserved through this process as the combined energy and momentum of an entangled photon pair are the same as those of a pump photon. The twin photons can exit the nonlinear crystal at different times that are dictated by the time needed to propagate the length of the crystal. Entanglement time  $(T_e)$  is the largest estimate of this range of times, as dictated by the dimensions of the crystal, which can be further tuned by placing a quartz plate to adjust the refractive index of the medium. More accurately,  $T_e$  is determined by the width of the fourth-order temporal coherence function of the entangled photon pair.<sup>20</sup> In addition to the temporal coherence, polarization entanglement is produced for the photon pairs generated using SPDC. Among two types of SPDC processes (type-I and II), type-II SPDC generates perpendicularly polarized photon pairs using a BBO ( $\beta$ -barium borate) crystal. Recently entangled photons from the type-II SPDC process have been extensively applied to the study of various two-photon absorbing chromophores by Goodson and co-workers. 21-25 In these works, the correlated photon pairs arrive at the absorbing medium with a flux density,  $\phi_{\rm e}$ , per photon pair (photons cm<sup>-2</sup> s<sup>-1</sup>). The overall ETPA rate, R<sub>e</sub>, is known to be linearly dependent on the input flux:<sup>21,22,24,26</sup>

$$R_{\rm e} = \sigma_{\rm e} \phi_{\rm e} \tag{1}$$

where  $\sigma_{\rm e}$  is the ETPA cross section. The ETPA cross sections are reported on the order of  $10^{-17}$  cm<sup>2</sup> using low photon fluxes ( $10^{12}$  photons cm<sup>-2</sup> s<sup>-1</sup>). The cross sections are many orders of magnitude higher than those which would be obtained from TPA using high photon fluxes ( $10^{22}$  photons cm<sup>-2</sup> s<sup>-1</sup> ×  $10^{-48}$  cm<sup>4</sup> s =  $10^{-26}$  cm<sup>2</sup>).  $^{21-24}$ 

There have been a few theoretical studies in which ETPA cross sections were evaluated for atoms and small molecules. Fei et al. derived a Kramers-Heisenberg-like expression for the ETPA cross section expression for the first time and used it to obtain the ETPA cross section of atoms. 26,27 Recently, Burdick et al. have provided detailed quantum chemical descriptions of ETPA for diatomic molecules.<sup>28</sup> In addition, extensive work to simulate the frequency-resolved absorption of model systems by entangled photons through a pump-probe scheme has been proposed by the Mukamel group. 29-31 Although these previous theoretical studies provided meaningful insights for understanding ETPA for model systems, a quantitative description of entangled photon interactions with large organic chromophores has been lacking, yet it is important for understanding the applicability of ETPA. In addition, future experiments may be able to better control the entanglement beam parameters based on a detailed understanding of entangled photon generation, including sources other than SPDC. 32,33 Since the electronic structure of a molecule becomes more complicated with increasing size of the molecule, a systematic and efficient approach to obtain ETPA cross sections is required.

Motivated by the above discussion, we use a recently developed approach<sup>34,35</sup> called second linear response time-dependent density functional theory (SLR-TDDFT), in combination with a new approach to the determination of line shape functions for entangled photons, to calculate both TPA and ETPA cross sections, and to make quantitative comparisons with experiment for large organic molecules. SLR-TDDFT is an extension of traditional linear response TDDFT for the description of excited state properties, including transition multipoles and permanent dipole moments involving

excited states. SLR-TDDFT is in principle exact (in practice approximate depending on the choice of exchange-correlation approximation). Formally it involves examining the response of the initial state of the system to a weak external perturbation. This analysis is performed in the linear response regime. SLR-TDDFT is a different approach with respect to standard (linear response) TDDFT as the latter refers to excitations only from the ground electronic state of the molecule being studied. SLR-TDDFT is designed to rigorously determine transition moments between two excited states by doing two calculations, first a conventional TDDFT (ground state) calculation, and then a second in which the initial state is described by the ground state plus a small amount of the excited state of interest. There are other ways to calculate transition moments between different excited states, such as quadratic TDDFT, however SLR-TDDFT has superior scaling properties that are useful for the large molecules being studied in this work. An advantage of the SLR-TDDFT algorithm is that the energy spectrum obtained from standard (or first) linear response TDDFT can be used to compute the excited-state-to-excitedstate excitation frequencies, so if the energy spectrum is accurate so are spectroscopic properties. Furthermore, in the algorithm developed by Mosquera et al., 34 the calculation of a single excited state has the same cost of a standard LR-TDDFT computation, thus offering computational advantages to the calculation of the ETPA and TPA cross sections for large molecules.

In this work, we apply SLR-TDDFT to the efficient calculation of TPA and ETPA cross sections for thiophene dendrimers, making comparison with experimental results which have been determined previously. In addition, we describe methods for determining the line shape functions for TPA and ETPA (needed for evaluating cross sections) in which we take into account the different excited state densities associated with classical and entangled excitation. We justify this analysis by examining the quantum electrodynamics of a three level model of ETPA, where we show that high degrees of entanglement arise when the radiative lifetime of the twophoton excited state is much smaller than that for the onephoton excited states that serve as intermediates in ETPA. The calculated cross sections show good agreement with the experimental values, indicating the accuracy of both our SLR-TDDFT approach and our model for estimating line shapes. Further, we provide a state-resolved analysis of the interference patterns in the ETPA cross section over varying entanglement time, and show that the quantum light source provides new information about molecular electronic states that is not available with classical photons.

## **■ THEORETICAL DETAILS**

Classical Two-Photon Absorption Cross Section. The TPA cross section for a classical two-photon source,  $\delta_v$  is given by the following equation under near-resonance conditions:  $^{36-38}$ 

$$\delta_r = \frac{\pi}{2} \omega_1 \omega_2 \langle S_r^2 \rangle g_r(\omega_0, \Gamma)$$
 (2)

where  $\omega_1$  and  $\omega_2$  are the signal and idler frequencies, respectively. In most TPA and ETPA measurements, the frequencies of the two sources are degenerate ( $\omega_1 = \omega_2 = \omega_p/2$ ).  $g_r(\omega_0, \Gamma)$  is the line shape function for excitation by classical photons. The line shape broadening is determined by the excited state damping factor  $\Gamma$  and is often chosen to be 0.1

eV for TPA, corresponding to the measured two-photon line shape for many molecules.<sup>38–41</sup> Later we show that this choice of damping factor provides reasonable quantitative agreement between measured and calculated cross sections, but one could argue that values larger or smaller by a factor of 2 could also have been used, indicating the level of uncertainty of our results (consistent with previous work<sup>42</sup>). Here we assume a Lorentzian line shape function for  $g_r(\omega_0, \Gamma)$ :<sup>38</sup>

$$g_r(\omega_0, \Gamma) = \frac{1}{\pi} \frac{\Gamma}{(\omega_1 + \omega_2 - \omega_0)^2 + \Gamma^2}$$
 (3)

Under the two-photon resonance condition,  $g_r(\omega_0, \Gamma) = 1/\pi\Gamma$ . If the half width is 0.1 eV, then the resulting line shape function yields a value of 13 fs for the effective excited state lifetime.  $\langle S_r^2 \rangle$  is the rotationally averaged TPA strength in the molecular coordinate to account for ensemble averaging in bulk samples. This term is expressed as a sum of two-photon transition matrix elements  $S_{r,\mathrm{ab}}$  with polarization-dependent parameters  $(F,G,\mathrm{and}\ H)$ :

$$\langle S_r^2 \rangle = \frac{1}{30} \sum_{ab} \left( F S_{r,aa} \overline{S}_{r,bb} + G S_{r,ab} \overline{S}_{r,ab} + H S_{r,ab} \overline{S}_{r,ba} \right) \tag{4}$$

For linearly polarized light with parallel polarization, F = G = H = 2, whereas F = H = -1 and G = 4 for perpendicularly polarized light. In the experiment, parallel polarization is generally used for classical TPA measurements whereas perpendicular polarization generated through the type-II SPDC process is used for ETPA measurements. The classical two-photon transition probability between the initial state  $|i\rangle$  and final state  $|f\rangle$ ,  $S_{ab}$ , is expressed as the following sum-overstates expression:

$$S_{r,ab}^{if} = \sum_{j} \left[ \frac{D_{ab}^{(j)}}{\Delta_{1}^{(j)} - i\kappa_{j}/2} + \frac{D_{ba}^{(j)}}{\Delta_{2}^{(j)} - i\kappa_{j}/2} \right]$$
(5)

where  $\kappa_i$  is a phenomenological line width of the intermediate state |i| which can be considered a constant for a sufficiently weak photon-flux density. This is also referred to as a dephasing factor due to various effects including vibronic and solvent effects. Because of the technical difficulty in accurately obtaining the value both experimentally and theoretically, we will study the cases, where (1)  $\kappa_i$  is zero and (2) has a commonly accepted upper limit which is 0.1 eV. Later in this work, we conclude that the cross sections are not sensitive to to this range of values of  $\kappa_i$ . The transition matrix element with the molecular electric dipole moment components in the molecular coordinates is given by  $D_{ab}^{(j)} = \langle f | \mu_b | j \rangle$ (j)  $\mu_a$  | i). Energy mismatches are defined as  $\Delta_1^{(j)} = \epsilon_i - \epsilon_i - \omega_1$ and  $\Delta_2^{(j)} = \epsilon_j - \epsilon_f + \omega_2$ , where the phase matching condition is  $\omega_p = \omega_1 + \omega_2$ . Note that the denominators in the first and the second summation terms of the transition matrix element are identical only if the energy sum of the signal and idler photons is resonant with the energy difference between the final and initial states:  $\epsilon_f - \epsilon_i = \omega_1 + \omega_2$ . One should note that the transition probability for either entangled or unentangled absorption does not necessarily require a summation over molecular electronic states; instead, these molecular states provide a convenient expansion for the virtual states that are the intermediates. However, we have adopted the sum-overstates formulation derived by Teich and co-workers 26,27 for the purpose of providing a practical tool for probing the molecular electronic structure in this work. Especially for ETPA, this

formalism is found to provide a rapidly converging representation of the virtual states, including interferences that arise from the entangled photons. Also, we assume the electronic resonance condition in which both energy mismatch expressions can be generalized as  $\Delta_k^{(j)} = \epsilon_j - \epsilon_i - \omega_k$ . The terms inside the brackets of the above transition probability element are summed over all electronic states including the ground and final states  $(j \geq i)$ . Under the two-photon resonance condition with degenerate photon energies, eq 5 reduces to the following form:

$$S_{r,ab}^{if} = 2 \sum_{j} \frac{D_{ab}^{(j)}}{\Delta^{(j)} - i\kappa_{j}/2} = \sum_{j} \beta_{ab}^{(j)}$$
(6)

In eq 6, we introduced a single-state transition probability element,  $\beta_{ab}^{(j)}$ , to resolve the role of each intermediate state and the interaction among multiple states.

**Entangled Two-Photon Absorption Cross Section.** The ETPA cross section was determined quantum mechanically for a time-entangled twin state wave packet. Analogous geometrical considerations used in the simplified probabilistic model yield the following expression for the ETPA cross section:

$$\sigma_{e} = \frac{\pi}{4A_{e}T_{e}}\omega_{1}\omega_{2}\langle S_{e}^{2}\rangle g_{e}(\omega_{f})$$
(7)

where  $A_e$  is the entanglement area which we assume has the value  $A_e=10^{-6}~{\rm cm}^2$  based on previous work with SPDC sources. Te is the entanglement time between the photon pairs which is determined by the experimental setup within the range of 50–100 fs. The line shape function for ETPA is  $g_e(\omega_f)$  which will be discussed in detail below. We assume that the entangled photon pairs are created by parametric type-II down-conversion, where the polarization of the signal photon is orthogonal to that of the idler photon. Using second-order time-dependent perturbation theory with an entangled twin state yields the following transition probability matrix element from the ground state  $|i\rangle$  to the final excited state  $|f\rangle$ :

$$S_{e,ab}^{ij} = \sum_{j} \left[ D_{ab}^{(j)} \frac{1 - \exp[-iT_{c}\Delta_{1}^{(j)} - T_{c}\kappa_{j}/2]}{\Delta_{1}^{(j)} - i\kappa_{j}/2} + D_{ba}^{(j)} \frac{1 - \exp[-iT_{c}\Delta_{2}^{(j)} - T_{c}\kappa_{j}/2]}{\Delta_{2}^{(j)} - i\kappa_{j}/2} \right]$$
(8)

Using  $\beta_{ab}^{(j)}$  defined in eq 6, the above expression can be reduced to the following:

$$S_{e,ab}^{if} = \sum_{j} \beta_{ab}^{(j)} [1 - \exp[-iT_e \Delta^{(j)} - T_e \kappa_j / 2]]$$
(9)

Three parameters dependent on the choice of intermediate state  $|j\rangle$  are included in this expression: the transition matrix element  $D^{(j)}$ , the energy mismatch  $\Delta^{(j)}$  and the line width of the state  $\kappa_j$ . The strengths of the transition matrix elements and the transition symmetry are critical in determining  $D^{(j)}$ , as this depends on the dot product of two transition elements. The excited state energies relative to the excitation energy are determined by  $\Delta^{(j)}$ . Since the evaluation of  $\kappa_j$  is not straightforward for molecules with large numbers of degrees of freedom, we assume a constant line width parameter in this work. Although the entanglement time  $T_e$  is not a material dependent factor (it depends on the source properties), the variation in the ETPA cross section on  $T_e$  will be also considered due to uncertainty in its value.

**ETPA Line Shape.** It is important to emphasize that the line shape for ETPA,  $g_e$ , is different from the classical TPA line shape function,  $g_r$ . The line width associated with  $g_r$  is associated with rapid dephasing of the two-photon excited state by any process, while that for  $g_e$  reflects decay via entangled photons. There are certain excited states of atoms where these two line widths can be the same, so previous studies of atomic systems have not considered this issue, but in the present case the differences are many orders of magnitude. To understand how this works, we consider two-photon excitation in the three-level model shown in Figure 1. In this

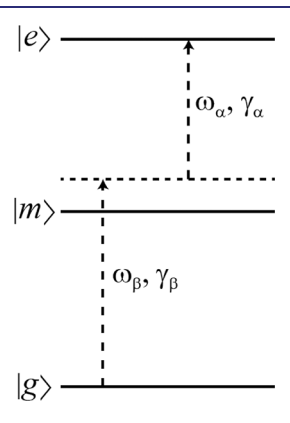


**Figure 1.** Three-level model used for the description of two-photon absorption. The molecule initially is in its ground state and may absorb a photon with excitation energy  $\omega_{\beta}$  and absorption rate  $\gamma_{\beta}$ , followed by the absorption of a second photon with excitation energy  $\omega_{\alpha}$  and rate  $\gamma_{\alpha}$ .

model, the molecule in its ground state may absorb a photon with excitation energy of  $\omega_{\beta}$  and absorption rate  $\gamma_{\beta}$ , followed by absorption of a second photon with excitation energy of  $\omega_{\alpha}$  and rate  $\gamma_{\alpha}$ . In this version of the analysis we consider unentangled photons. The interaction Hamiltonian, in the rotating-wave approximation, for this system is expressed as follows:

$$\hat{H}_{I} = \hbar g_{\alpha}^{*} \hat{\psi}_{me}^{\dagger} \hat{\mathbf{a}} e^{-i\Omega_{\alpha}t} + \hbar g_{\beta}^{*} \hat{\psi}_{gm}^{\dagger} \hat{\mathbf{a}} e^{-i\Omega_{\beta}t} + \text{H.c.}$$
(10)

where  $\omega - \omega_i = \Omega_i$ . The molecule-field couplings in the dipole approximation are given by  $g_{\alpha}^* = \langle \mu_{me} \cdot \mathbf{E}(\mathbf{r}) \rangle$  and  $g_{\beta}^* = \langle \mu_{gm} \cdot \mathbf{E}(\mathbf{r}) \rangle$ , where  $\mu_{me}$  and  $\mu_{gm}$  are the corresponding dipole matrix elements and  $\mathbf{E}(\mathbf{r})$  is the electric field interacting with the system. It should be noted that the coupling matrix elements are assumed to be averaged over all possible orientations. The transition operators for the absorption scheme shown in Figure 1 are defined by the following:

$$\begin{split} \hat{\psi}_{me}^{\dagger} &= |e\rangle\langle m|, \, \hat{\psi}_{gm}^{\dagger} = |m\rangle\langle g| \\ \hat{\psi}_{me} &= |m\rangle\langle e|, \, \hat{\psi}_{gm} = |g\rangle\langle m| \end{split} \tag{11}$$

The overall set of basis functions is given by  $|0\rangle \otimes |g\rangle$ ,  $|0\rangle \otimes |m\rangle$ , and  $|0\rangle \otimes |e\rangle$  and we use this basis to construct the interaction Hamiltonian,

$$\hat{H}_{I} = \hbar \begin{pmatrix} 0 & g_{\beta}e^{i\Omega_{\beta}t} & 0 \\ g_{\beta}^{*}e^{-i\Omega_{\beta}t} & 0 & g_{\alpha}e^{i\Omega_{\alpha}t} \\ 0 & g_{\alpha}^{*}e^{-i\Omega_{\alpha}t} & 0 \end{pmatrix}$$

$$(12)$$

Given this Hamiltonian, the time evolution of the density matrix is specified by the Liouville equation as follows:

pubs.acs.org/JACS

$$\frac{\partial \rho_{ij}}{\partial t} = -\frac{i}{\hbar} \sum_{k} \left( H_{ik} \rho_{kj} - \rho_{ik} H_{kj} \right) - \left( \gamma \rho_{ij} - \rho_{ij} \gamma_{j} \right) \tag{13}$$

where we include for the relaxation of each state using  $\langle i| \hat{\gamma} | j \rangle = \gamma_i \delta_{ij}$ . The decay rates of the populations of the first and second excited states will be denoted  $\gamma_{\alpha}$  and  $\gamma_{\beta}$ , respectively. It should be noted that here have not included dephasing in eq 13 (as can be done using the Lindblad equation) so as to simplify the analysis. In order to obtain the solution to these equations of motion, it is more convenient to reformulate it using the transition operators  $\rho_{ij}(t) = \hat{\phi}_i(t)\hat{\phi}_i^*(t)$  as follows:<sup>44</sup>

$$\frac{\partial \hat{\phi}_{i}(t)}{\partial t} = -\frac{i}{\hbar} \sum_{j} H_{ij} \hat{\phi}_{j}(t) - \gamma_{i} \hat{\phi}_{i}(t)$$
(14)

which can be simplified in a matrix form,

$$\begin{pmatrix} \dot{\phi}_{g} \\ \dot{\phi}_{m} \\ \dot{\phi}_{e} \end{pmatrix} = \begin{pmatrix} -i\omega_{g} & -ig_{\beta} & 0 \\ -ig_{\beta}^{*} & -(\gamma_{\beta} + i\omega_{m}) & -ig_{\alpha} \\ 0 & -ig_{\alpha}^{*} & -(\gamma_{\alpha} + i\omega_{e}) \end{pmatrix} \begin{pmatrix} \phi_{g} \\ \phi_{m} \\ \phi_{e} \end{pmatrix}$$

$$(15)$$

With no further approximations, the above coupled set of equations can be solved numerically. However, it is more instructive and sufficiently accurate at low intensities to assume that we are in a weak interaction regime so that the population of the intermediate state does not change over time, i.e.,  $\dot{\phi}_m = 0$ , therefore we have the following:

$$\phi_{m} = -\frac{ig_{\beta}^{*}}{\gamma_{\beta} + i\omega_{m}}\phi_{g} - \frac{ig_{\alpha}}{\gamma_{\beta} + i\omega_{m}}\phi_{e}$$
(16)

Substituting the above expression in eq 15 and diagonalizing the matrix, the general solution for this set of differential equations with the initial condition of  $\rho_{ee}(t=0)=\rho_{mm}(t=0)=0$  and  $\rho_{ee}(t=0)=1$ , is given by:

$$\rho_{gg}(t) = \phi_{g}(t)\phi_{g}^{*}(t) = e^{-2\theta t}, \quad \text{where } \theta = \frac{\gamma_{\beta}|g_{\beta}|^{2}}{\gamma_{\beta}^{2} + \omega_{\beta}^{2}}$$

$$\rho_{ee}(t) = \phi_{e}(t)\phi_{e}^{*}(t) = K_{e}[e^{-2\gamma_{\alpha}t} - 2e^{-(\gamma_{\alpha}+\theta)t}\cos(\omega_{\beta}t) + e^{-2\theta t}]$$
(17)

where,

$$K_{\epsilon} = \frac{\left|g_{\alpha}g_{\beta}\right|^{2}}{\left(\omega_{\alpha}\omega_{\beta} + \omega_{\beta}^{2} + \gamma_{\alpha}\gamma_{\beta} - \left|g_{\beta}\right|^{2}\right)^{2} + \left(\omega_{\alpha}\gamma_{\beta} + \omega_{\beta}\gamma_{\beta} + \omega_{\beta}\gamma_{\alpha}\right)^{2}}$$

We obtained the above expressions assuming  $\omega_g = 0$ ,  $\omega_m = \omega_{\beta}$ , and  $\omega_e = \omega_{\alpha} + \omega_{\beta}$ . Note that here  $\rho_{gg}$ ,  $\rho_{mm}$ , and  $\rho_{ee}$  are the density of ground, intermediate and excited states, respectively. We see that the excited state probability  $\rho_{ee}(t)$  involves the competition between two time scales, one determined by  $\gamma_{\alpha}$  and the other by  $\theta$ . Here  $\theta$  is determined by the pumping rate to the intermediate state. If this is fast enough, then the time dependence of  $\rho_{ee}$  is governed by  $\theta$ . Alternatively for slower pumping,  $\gamma_{\alpha}$  determines the time scale for populating the excited state. Below we show that the parameters relevant to the present work are where  $\gamma_{\alpha}$  dominates. We may determine the ground and excited state densities in the frequency domain for a more advanced analysis,

$$\rho_{gg}(\omega) = \frac{4\theta}{4\theta^2 + (\omega - \omega_{\beta})^2}$$

$$\rho_{ee}(\omega) = \frac{4\gamma_a}{4\gamma_a^2 + (\omega - \omega_a)^2} - \frac{2(\gamma_a + \theta)}{\omega_{\beta}^2 + (\gamma_a + \theta)^2 + (\omega - \omega_a)^2}$$

$$+ \frac{4\theta}{4\theta^2 + (\omega - \omega_a)^2}$$
(18)

In Figure 2 we plot  $\rho_{gg}$  and  $\rho_{ee}$  as a function of frequency using parameters discussed later for the planar 6T molecule. This

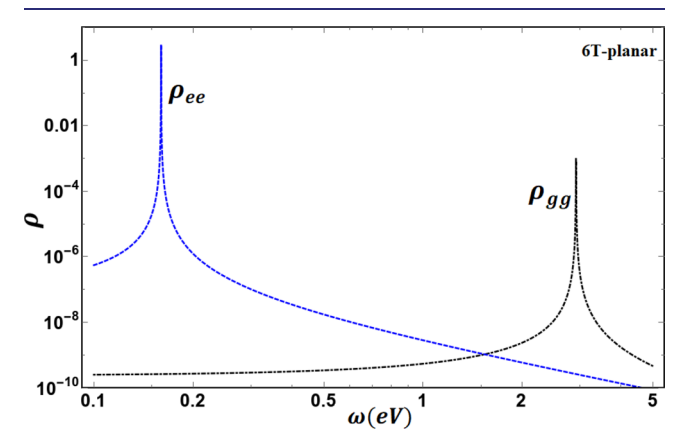


**Figure 2.** Population of ground and two-photon excited states for the three-level model. In the calculations, we used the values in Tables 1 and 3 for the excitation energies of 6T-planar  $(\omega_{\alpha}, \omega_{\beta})$ , and the widths  $\gamma_{\alpha} = 0.001$  and  $\gamma_{\beta} = 1.6$  MHz.

shows the extremely narrow line shape for  $\rho_{ee}$  near  $\omega=\omega_{\alpha}$  that arises using the small value of  $\gamma_{\alpha}$  that results from the SLR-TDDFT calculations.

In the Supporting Information (SI), we present a similar analysis of the Liouville equation within the context of quantum electrodynamics, as applied to emission process starting from the two-photon excited state. In this case, the emission line width is determined by the second order frequency correlation function of the emitted photons:

$$g_{\times}^{(2)}(\omega) \approx \gamma_{\alpha} \gamma_{\beta} \left( \gamma_{\beta} - 1 \right) \frac{1}{(\omega - \omega_{\alpha} - \omega_{\beta})^{2} + \gamma_{\alpha}^{2}} \times \frac{1}{(\omega - \omega_{\beta})^{2} + \gamma_{\beta}^{2}}$$

$$(19)$$

The width of resonances in this correlation function, which determines the characteristic width of the frequency anticorrelation, is governed by  $\gamma_{\alpha}$  as long as  $\gamma_{\alpha} \ll \gamma_{\beta}$ . The spectra associated with  $g_{\chi}^{(2)}$  are plotted in Figure S2 using the calculated values for the molecules of interest in this work. Note that two sharp peaks are associated with the emission process. The peaks represent the detection of one and two emitted photons where the width corresponding to the two-photon process is much narrower than that of the one-photon process. Therefore,  $\gamma_{\alpha}$  can be interpreted as a width factor while it is the emission rate of the first photon. We also note that  $\gamma_{\alpha} \ll \gamma_{\beta}$  is required for producing a highly entangled state (large Schmidt number) in two-photon emission.

We conclude that the width  $\gamma_a$  of the two-photon state  $\rho_{ee}$  shows up equivalently in both the absorption and emission processes. We note that this use of the spontaneous radiative emission lifetime of the two-photon excited state to determine the line width for the ETPA cross section was used previously for the OH molecule.<sup>46</sup> In the present applications, we

determined the ETPA line shape using the spontaneous radiative lifetime from Fermi's golden rule:

$$g_{e}(\omega_{f}) = \tau_{r} = \left[ \sum_{j < f} \frac{4}{3\hbar} \left( \frac{|\omega_{jf}|}{c} \right)^{3} |\mu_{jf}|^{2} \right]^{-1}$$
(20)

based on results for the two-photon excited state from the SLR-TDDFT calculations. In addition, we have verified from our calculations that the two-photon allowed excited state has a much longer radiative lifetime than the intermediate states produced after emission of the first photon. Due to this huge difference in lifetimes, two-photon absorbing dyes are an ideal system for maximum ETPA efficiency.

#### COMPUTATIONAL DETAILS

The geometries of the molecules investigated in this work were first optimized with the B3LYP hybrid functional and the 6-31G\* basis set. This same level of theory was used for the excited state calculations, as for 18T this is the highest level that is feasible with the facilities available to us. For each molecule, a SLR-TDDFT calculation was carried out to generate the 15 lowest-lying excited states. DFT and TDDFT calculations were performed using the NWChem computational package version 6.6 modified by Mosquera et al. to calculate oscillator strengths and transition dipole matrix elements for intraband transitions between two excited states. 34,35 In this approach, the intraband transition dipoles are effectively calculated by running two steps of TDDFT. In the first step, a standard linear response TDDFT calculation is run, and the ground state orbitals are redefined as follows (the Tamm-Dancoff approximation is used here):

$$\begin{split} & \varphi_{i\sigma}(\mathbf{r}) & \leftarrow \varphi_{i\sigma}(\mathbf{r}) + \lambda \sum_{a} X_{ai\sigma}^{I} \varphi_{a\sigma}(\mathbf{r}) \\ & \varphi_{a\sigma}(\mathbf{r}) & \leftarrow \varphi_{a\sigma}(\mathbf{r}) - \lambda \sum_{i} X_{ai\sigma}^{I} \varphi_{i\sigma}(\mathbf{r}) \end{split} \tag{21}$$

where the indices i and a denote occupied and virtual orbitals, respectively,  $\sigma$  denotes the z-spin,  $X_{ai\sigma}^I$  is the excitation vector from standard TDDFT for the excited state labeled I, and  $\lambda$  is a small number (in spin-restricted calculations we set  $\varphi_{p,\uparrow}=\varphi_{p,\downarrow}$ ). These new orbitals, with the exact XC potentials, could represent the density of the linear combination  $\Psi_0+\lambda\Psi_D$  where  $\Psi_0$  is the true ground-state wave function, and  $\Psi_I$  is the true excited state of interest. With the redefined orbitals, the LR-TDDFT equations are solved once again, and the transition dipoles of the perturbed and original LR-TDDFT calculations are compared. In ref 34 we showed that the numerical derivative:

$$\mathbf{d}_{J,I} = \frac{\mathbf{d}_{J,0}(\lambda) - \mathbf{d}_{J,0}(\lambda = 0)}{\lambda} \tag{22}$$

can be used to compute the transition dipole  $(\mathbf{d}_{J,I})$  for the excitation from state I to state J (where J is in a chosen energy window). In the above equation,  $\mathbf{d}_{J,0}$  denotes the transition dipoles for excitation from the reference to the state labeled J. On the basis of our previous calculations on oligomers of polythiophene, <sup>35</sup> we determined that  $\lambda = 10^{-2}$  is appropriate for calculations of the above derivative (the results do not change significantly by further reducing this value). The SLR-TDDFT calculation yields a new family of excitation vectors, which we refer to as SLR vectors. However, if some roots are

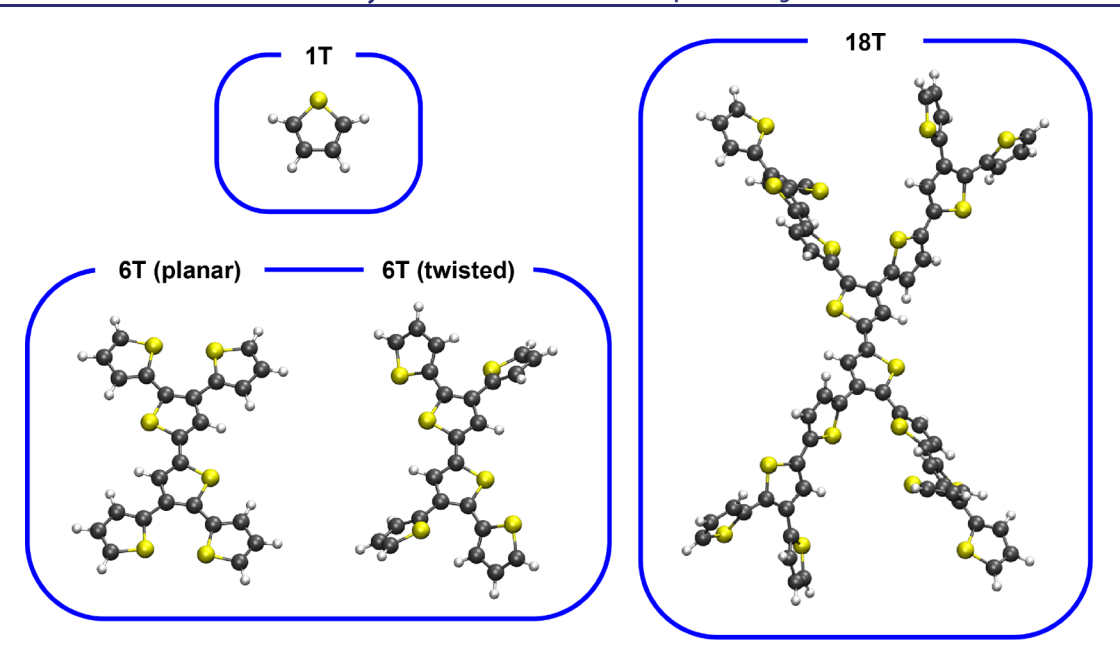


Figure 3. DFT optimized structures of thiophene dendrimers with 1, 6, and 18 thiophene monomers. Two different conformers of the 6T molecule were optimized with planar and twisted geometries (white: hydrogen; gray: carbon; and yellow: sulfur).

degenerate, then the SLR-TDDFT calculation can slightly break the degeneracy, and the SLR vectors have to be rematched with their first LR counterparts. To reorganize the roots, we used the following criterion: a first linear response vector  $\mathbf{X}$  and an SLR vector  $\overline{\mathbf{X}}$  correspond to one another if  $1-C_r < |\mathbf{X} \cdot \overline{\mathbf{X}}| < 1+C_r$ . We use the value  $C_r = 0.05$ . We thus have two sets of transition dipoles, one for the ground-state reference, and another for the perturbed reference, constructed with the formula shown in eq 22; these transition dipoles are computed using the first and second LR excitation vectors, respectively. Once the transition dipoles are obtained, both TPA and ETPA cross sections were calculated using a homebuilt Python code.

## ■ RESULTS AND DISCUSSION

In order to study a model system to obtain TPA and ETPA cross sections, structures of thiophene monomer (1T) and two thiophene dendrimers with 6 and 18 monomers (6T and 18T) were optimized using DFT and the corresponding optimized geoemetries are shown in Figure 3. These thiophene dendrimers were selected because experimental measurements on both TPA and ETPA cross sections were reported by the Goodson group.<sup>22</sup> 1T was not experimentally studied, but we included this molecule for comparison. These molecules can serve as a good model system due to structural simplicity as well as chemical similarity among the molecules as dictated by the thiophene unit. Two structural conformers of 6T were generated so as to test the effects of a torsional geometry change and changes in delocalization of the  $\pi$  electrons on the results. The planar structure in which all atoms are positioned in a single plane is more energetically stable by 29 meV than the twisted structure. However, the thermodynamic barrier between the two structures is small enough for 6T to undergo dynamic structural evolution between different conformers at room temperature. The same issue arises for 18T, but to keep the calculations manageable we will only consider the structure presented in Figure 3.

Absorption spectra of thiophene dendrimers were first simulated to estimate the optically allowed transitions and compare them to UV—vis spectra. In Figure 4, the absorption

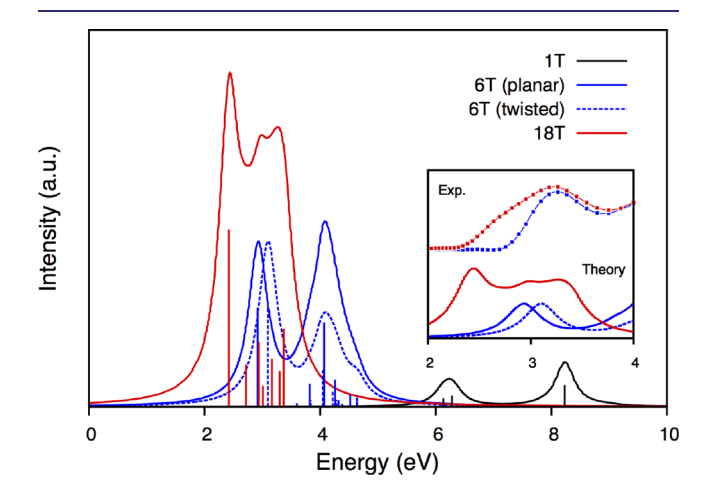


**Figure 4.** Calculated absorption spectra of 1T (black), 6T (blue), and 18T (red) using LR-TDDFT. The vertical lines indicate positions and oscillator strengths of excitation. Experimental absorption spectra are shown in the inset as a comparison.  $^{22}$ 

peaks are broadened using a Lorentzian broadening function with a full-width half-maximum (FWHM) of 0.1 eV. The simulated spectra are compared with the previously reported experimental absorption spectra. As shown in the simulated spectra, the first absorption bands at 2.92 and 3.10 eV, corresponding to planar and twisted 6T, respectively, match well with the experimental peak at 3.2 eV. The torsional twist in 6T slightly blue-shifts absorption energies as a result of the reduced planar  $\pi$ -conjugated structure, as expected. However, the small twist in the geometry does not impact the optical transitions significantly. The major absorption peak for 18T experimentally observed at 3.2 eV is likely due to the peaks in the range of 2.7 to 3.1 eV. Also, the first absorption peak at 2.42 eV can be matched with the shoulder peak at  $\sim$ 2.7 eV in

Table 1. Transition Energy, Dipole, and Oscillator Strength for the Ten Lowest Singlet Transitions of 6T and 18Ta

	6T (planar)			6T (twisted)			18T		
no.	energy (eV)	$\mu^{i  o f}$ (a.u.)	$f^{i  o f}$	energy (eV)	$\mu^{i  o f}$ (a.u.)	$f^{i  o f}$	energy (eV)	$\mu^{i  o f}$ (a.u.)	$f^{i  o f}$
ES1	2.92	1.66, -3.45, 0.0	1.05	3.10	1.37, -3.49, -0.26	1.07	2.42	2.88, -4.83, -0.28	1.88
ES2	3.08	0.0, 0.0, 0.0	0.0	3.41	0.0, 0.0, 0.0	0.0	2.62	$0.0, \ 0.02, \ -0.02$	0.0
ES3	3.56	-0.01, $-0.01$ , $0.0$	0.0	3.65	0.0, 0.0, 0.0	0.0	2.72	0.01, 0.16, 0.02	0.0
ES4	3.60	-0.06, -0.65, 0.0	0.04	3.84	-0.14, -0.84, -0.02	0.07	2.72	-0.08, -2.59, 0.04	0.45
ES5	3.83	-1.25, 1.02, 0.0	0.24	4.03	0.0, 0.0, 0.0	0.0	2.82	0.01, -0.01, 0.01	0.0
ES6	3.83	-0.10, 0.11, 0.0	0.0	4.05	-0.86, -1.78, 0.08	0.39	2.94	-1.49, $-2.70$ , $0.11$	0.69
ES7	4.07	2.45, 1.72, 0.0	0.89	4.22	-1.18, $-0.49$ , $0.24$	0.17	3.01	-1.72, 0.19, 0.20	0.22
ES8	4.17	0.01, -0.01, 0.0	0.0	4.28	-0.35, 0.76, -0.07	0.07	3.03	-0.02, 0.0, 0.0	0.0
ES9	4.26	-0.69, -1.51, 0.0	0.29	4.31	0.0, 0.0, 0.0	0.0	3.11	-0.17, $-0.14$ , $0.05$	0.0
ES10	4.31	-0.13, -0.04, 0.0	0.0	4.38	-0.52, 0.04, -0.17	0.03	3.17	-0.47, 2.52, 0.09	0.51
and c									

<sup>a</sup>ES refers to excited state for each transition.

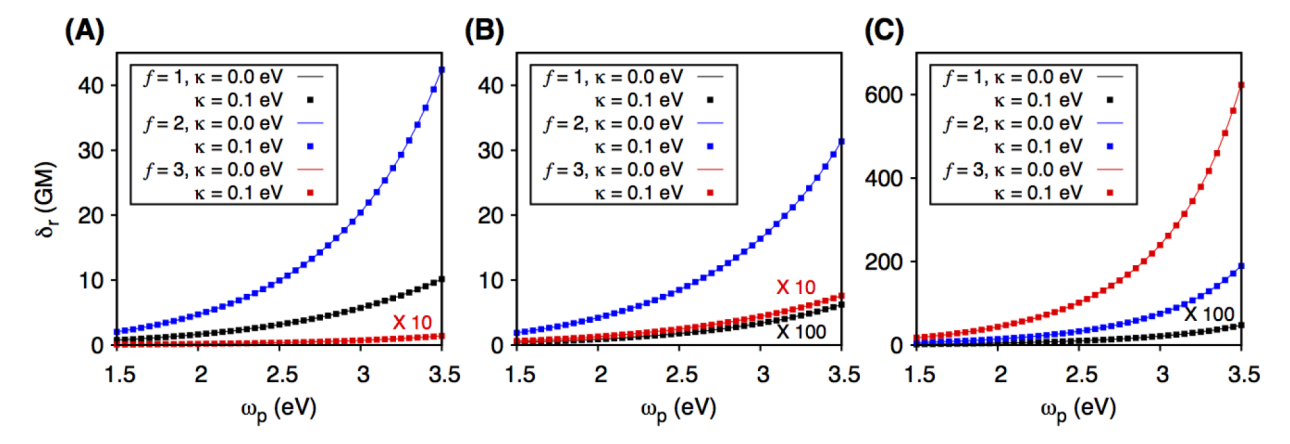


Figure 5. TPA cross section plots for (A) planar 6T, (B) twisted 6T and (C) 18T with three lowest excited states chosen as the two-photon excited state. Solid lines and squared dots represent cross sections with excited state line widths  $\kappa_j = 0.0$  and 0.1 eV, respectively.

the experiment. This shoulder peak is attributed to absorption by  $\alpha$ -thiophene chains of longer lengths within the dendron. Even though the TDDFT calculations are performed for isolated molecules, the simulated absorption spectra predict the energies for optically allowed transitions fairly well compared with the experiment carried out in solution. We also note that the absorption peaks of the thiophene monomer are located well above 6 eV, so dendrimer formation (and the expected delocalization of the  $\pi$  electrons) is important for meaningful two-photon absorption spectroscopy experiments. In Table 1, the energy, dipole moment, and oscillator strength of each transition for the ten lowest excited states of 6T and 18T are listed. The first transitions are dipole-allowed transitions with significant oscillator strengths for both molecules. Some calculated transitions are dipole-forbidden with zero dipole moment and not shown in the absorption spectra in Figure 4. However, these states play an important role in determining the TPA cross section as the transition symmetry is different for the two-photon process. Therefore, all excited states from both dipole-allowed and dipoleforbidden transitions were included in the cross section calculations.

In Figure 5, TPA cross sections for 6T and 18T are plotted as a function of pump energy  $\omega_p$ . Three cross sections are presented for each molecule, corresponding to choosing the first three excited states as the two-photon excited state. As expected from eq 2, a quadratic relationship between the TPA cross section and  $\omega_p$  is observed for both molecules. The quadratic relationship breaks if the intermediate state is

resonant for one photon excitation, however this is not the case for the molecules considered in this work. For both planar and twisted 6T, the second excited state (ES2), located at 3.08 and 3.52 eV, respectively, yields the highest TPA cross sections when it is chosen as the final state. (24 and 19 GM at  $\omega_n = 3.1$ eV for planar and twisted structures, respectively). When ES1 is chosen as the final state, the TPA cross section is smaller by a factor of 4 with a value of 6 GM for the planar structure. However, with ES2 as the final state, the TPA cross section becomes negligible for the twisted geometry. Regardless of the structure of 6T, the choice of ES3 as the final state shows a minimal effect in the TPA cross section. For 18T, the highest TPA cross section is found when ES3 is selected as the final state (288 GM at  $\omega_p$  = 3.1 eV). A negligible contribution by ES1 to the cross section is observed, whereas ES2 yields a meaningful cross section value of 90 GM. Note that the states yielding high TPA cross sections for every molecule are dipoleforbidden for one-photon transitions as shown in Table 1. The symmetry of each transition is visualized as a transition density in Figure S3. Although the transition densities from the ground state (GS) to ES1 for both 6T and 18T are localized along a linear dendrimer chain, they are distributed from one end of the molecule to the other. However, the two-photon allowed transitions for 6T (GS to ES2) are localized around the thiophene dimer moiety at the center, and this decreases the linearity of the transition density distribution. For 18T, the transition density is more delocalized over the dendrimer complex for two-photon allowed transitions (GS to ES2 and

ES3). This analysis indicates that assigning the final state for calculating the TPA cross section requires close attention.

The squared dots in Figure 5 show the trend in the TPA cross section with a finite line width value  $(\kappa_i)$  of 0.1 eV. Surprisingly, no significant difference in the cross section value with variation in  $\kappa_i$  was observed for any of the cases even though this value is toward the upper limit of typical line widths for organic molecules. This is because the energy mismatch  $\Delta_k^{(j)}$  in the denominator of the two-photon transition probability (eq 5) is much greater than  $\kappa_i/2$  unless a real state exists near the one photon energy. This infers that the existence of real states between the ground and the final states can impact the TPA cross section significantly. However, this condition does not apply to thiophene dendrimers and many organic chromophores as two-photon allowed states are usually higher in energy than the one-photon allowed state by a minimal amount. The TPA cross section values for the experimental excitation energy  $\omega_p = 3.1$  eV were calculated and are shown in Table 2. The comparison between experiment

Table 2. Comparison between Experimental<sup>22</sup> and Theoretical TPA Cross Sections for 6T and 18T<sup>a</sup>

	experiment <sup>22</sup>	theory		
molecule	$\delta_r (10^{-50} \text{ cm}^4 \text{ s})$	f	$\delta_r  (10^{-50}   \text{cm}^4   \text{s})$	
6T (planar)	6	ES2	24	
6T (twisted)	O	ES2	19	
18T	230	ES2	90	
		ES3	288	

<sup>a</sup>Theoretical cross sections were calculated with  $\omega_p = 3.1$  eV and  $\kappa_j = 0.0$  eV.

and theory shows excellent agreement (never worse than a factor of 4) for both 6T and 18T. The theoretical values slightly overestimate the TPA cross section, which could arise from a variety of factors including the existence of multiple structural conformers, intermolecular interactions, dielectric medium effects, issues with the choice of excited state line width, and errors in the SLR-TDDFT results.

In order to calculate the ETPA cross section  $\sigma_{\!\scriptscriptstyle{\mathcal{O}}}$  the final states chosen for the TPA cross section calculation (Table 2) were used. Calculated  $\sigma_e$  values as a function of the entanglement time  $T_e$  and pump energy  $\omega_p$  are shown as the colormap in Figure 6 for two values of the excited state line widths  $(\kappa_j = 0.0 \text{ (left)})$  and 0.1 eV (right)). As reported in previous works,  $\sigma_e$  oscillates with  $T_e$  due to the exponential in the cross section expression in eq 8. Since the oscillating nature of this formula originates from interference between the nonclassical photons and the electronic states of the molecule, detailed analysis of the pattern is desired. For both planar and twisted 6T (Figure 6A and B), one wave dominates the oscillation, with small distortions due to interference with other minor features. When the geometry is twisted, the ETPA cross section is attenuated as in the TPA case with shorter oscillation periods by 1-2 fs, regardless of  $T_e$ and  $\omega_v$ . Unlike 6T, multiple waves with slightly different oscillation periods are overlapped with each other for 18T with either ES2 or ES3 chosen as the final state (Figure 6C and D). The waves interfere all together and result in some irregular local maxima and minima in the cross section colormaps. Also, it is clear that longer oscillation periods are observed for 18T than for 6T. This is due to energy mismatch values  $(\Delta_k^{(j)})$  that are smaller for the larger molecule, as will be discussed later in

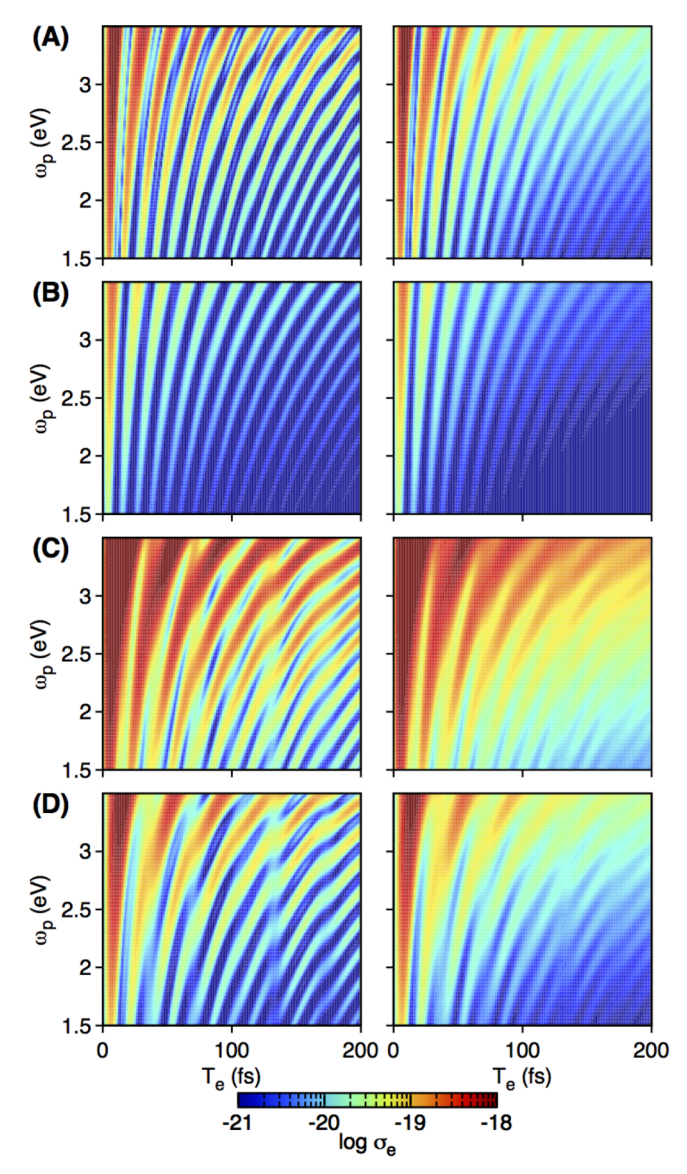


**Figure 6.** ETPA cross section  $(\sigma_e)$  colormaps as a function of  $T_e$  (x-axis) and  $\omega_p$  (y-axis) for (A) planar 6T (f = ES2), (B) twisted 6T (f = ES2), (C) 18T (f = ES2), and (D) 18T (f = ES3). The excited state line width is  $\kappa_j$  = 0.0 and 0.1 eV for the left and right colormaps, respectively. The colormaps are represented in the log scale of  $\sigma_e$ .

detail. Note that higher ETPA cross sections are obtained with ES2 than ES3 chosen as the final state. This is an unexpected result since the TPA cross section is higher by a factor of 3 when ES3 is the final state. Such discrepancy is due to the difference in the lifewidth for random and entangled TPA processes. As discussed in the Theoretical Details, the line width for the ETPA process is related to the radiative emission lifetime of the two-photon excited state, whereas that for random TPA (the 0.1 eV width) is assumed independent of the final state.

Calculated ETPA cross sections as well as line widths for chosen final states are listed in Table 3. Due to a large variation in the ETPA cross section, we chose local maximum values at  $\sim 100$  fs and  $\omega_p = 3.1$  eV in the colormaps for the comparison between experiment and theory. The excited state lifetime values (which determine the line width for ETPA) vary within the temporal range from 100 to 1000  $\mu$ s depending on the choice of the final state. These lifetimes are extremely long

Table 3. Comparison between Experimental and Theoretical ETPA Cross Sections for 6T and 18T<sup>a</sup>

	experiment <sup>22</sup>	theory				
molecule	$\frac{\sigma_{\epsilon}}{(10^{-19^{\epsilon}} \text{cm}^2)}$	f	$(10^{-19}$ cm <sup>2</sup> )	(µs)	$\gamma_f/\gamma_1$	
6T (planar)	1.3	ES2	1.7	988	$6 \times 10^{-4}$	
6T (twisted)	1.5	ES2	0.18	175	$3 \times 10^{-3}$	
18T	7.1	ES2	5.3	853	$6 \times 10^{-4}$	
		ES3	1.2	84	$6 \times 10^{-3}$	

<sup>&</sup>lt;sup>a</sup>Local maximum values at ~100 fs are chosen at  $\omega_p = 3.1$  eV in the colormaps in Fig. 6. ( $\kappa_i = 0.0$ ).

compared with typical one-photon excited state radiative lifetimes, due to the small frequency associated with transition between the intermediate state and the two-photon excited state. This is also supported by the obtained line width ratios of the final and the first excited states listed in Table 3 where we see  $\gamma_f \ll \gamma_1$  which is in line with our assumptions from the quantum electrodynamic analysis for the presence of a highly entangled state. The existence of a long-lived state excited by the entangled photon pair boosts the cross section significantly compared to the unentangled result. For 6T, the lifetime of the entangled two-photon excited state (ES2) becomes shorter for the twisted geometry, resulting in a decreased ETPA cross section. It is noticeable that ES2 results in a higher ETPA cross section than ES3 does for 18T due to the significantly longer lifetime value. This emphasizes that both the magnitude of the transition matrix element  $D_{ab}^{(j)}$  and the lifetime of the excited state induced by the entangled photons play critical roles in determining the ETPA cross section.

In addition to the wave-like features of the ETPA cross section, the dependence of cross section on the finite state line width  $\kappa_i$  is notable. A comparison between the left ( $\kappa_i = 0.0$ eV) and right ( $\kappa_i = 0.1$  eV) colormaps in Figure 6 shows the attenuation of the ETPA cross section with a finite value of  $\kappa_i$ . Without any changes in the oscillation pattern of the cross section, only the magnitude of the ETPA cross section decreases for a nonzero  $\kappa_i$ . This is in contrast to classical TPA in which the finite value of  $\kappa_i$  barely affects the cross section value. This is because of the presence of the dephasing factor in the exponential in eq 8, indicating that the transition probability is more sensitive to dephasing of the intermediate states when the two photons responsible for excitation are entangled. In addition, the ETPA cross section further decreases with increasing  $T_e$  for a nonzero  $\kappa_i$ . This is somewhat intuitive as the dephasing effect becomes more significant with increasing temporal coherence between the two photons. The correlation between  $\kappa_i$  and  $T_e$  in the ETPA cross section hints that even more detailed information such as vibronic features can be obtained using a source with a precise temporal resolution.

We now analyze the oscillating behavior of the ETPA cross sections in more detail. Specifically, it is essential to understand the relationship between the cross section behavior and the properties of each excited state. To do so, we used the single-state transition probability element suggested in eq 6 to distinguish the contribution from different intermediate states in the TPA cross section. Note that we used the classical TPA cross section values for the state-resolved analysis to ignore the dependence on the entanglement time and line width of the ETPA cross section. Since the TPA cross section is

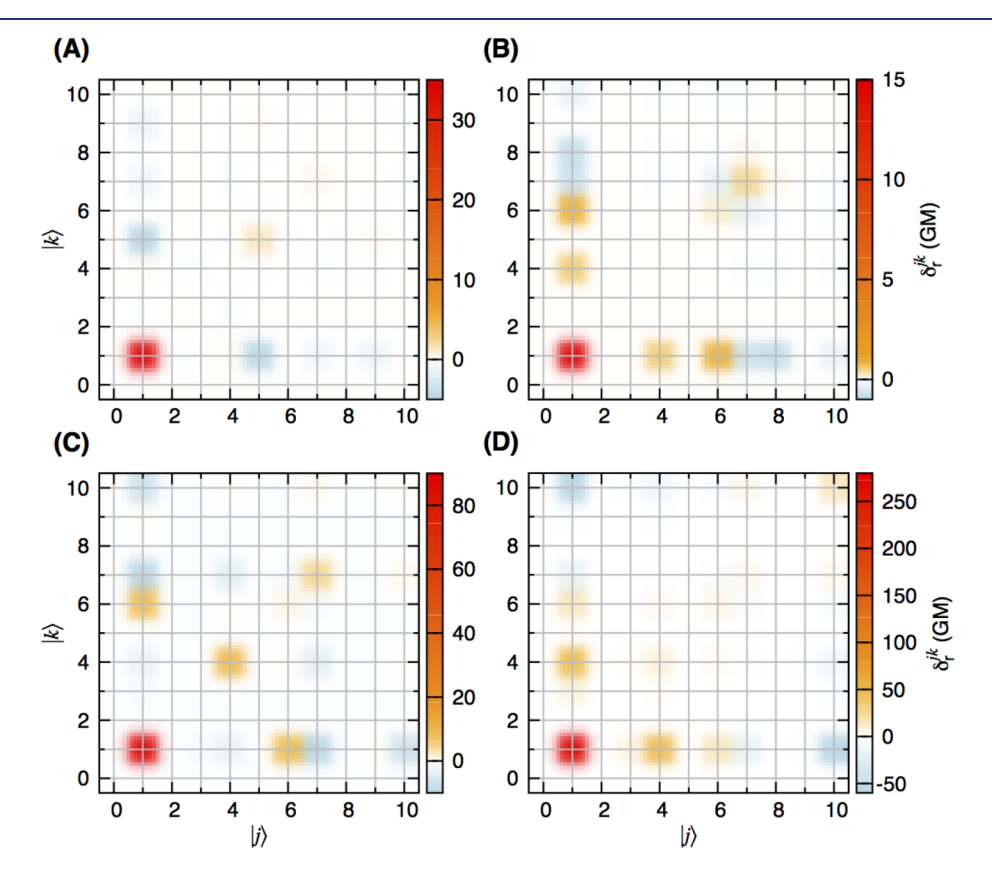
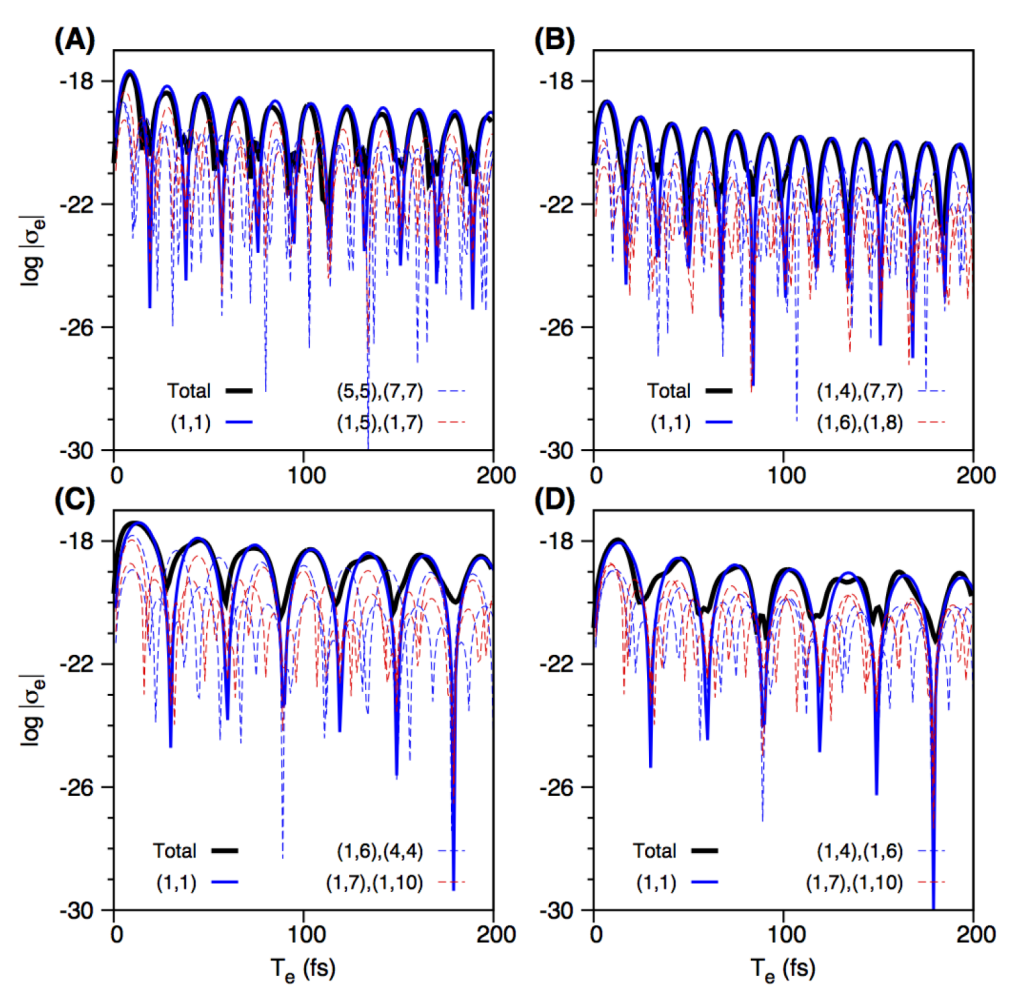


Figure 7. Distributions of fractional TPA cross section,  $\delta_r^{jk}$ , between states  $|j\rangle$  and  $|k\rangle$  for (A) planar 6T (f = ES2), (B) twisted 6T (f = ES2), (C) 18T (f = ES2), and (D) 18T (f = ES3). ( $\kappa_i$  = 0.0).



**Figure 8.** ETPA cross section plots for  $\omega_p = 3.1$  eV and  $\kappa_j = 0.0$  eV for (A) planar 6T (f = ES2), (B) twisted 6T (f = ES2) and (C) 18T (f = ES2), and (D) 18T (f = ES3). Bold black curve: total  $\sigma_e$  bold blue curve: major  $\sigma_e^{jk}$ , blue dashed curve: minor positive  $\sigma_e^{jk}$ , and red dashed curve: absolute value of minor negative  $\sigma_e^{jk}$ . The unit of  $\sigma_e$  is cm<sup>2</sup> and the y-value is plotted in a log scale for  $\sigma_e$ .

proportional to the square of the two-photon transition probability, it can be expressed as a double summation over the intermediate states:

$$\delta_r \propto \langle S_r^2 \rangle = \sum_{j,k} \langle \beta^{(j)} \beta^{(k)} \rangle \propto \sum_{j,k} \delta_r^{jk}$$
 (23)

The coupling between two intermediate states is included in the above expression, and a fractional TPA cross section  $\delta_r^{jk}$  is introduced which is dependent on the choice of two intermediate states. The fractional TPA cross section is positive when j = k, but can be negative otherwise. In Figure 7, couplings between states  $|j\rangle$  and  $|k\rangle$  are represented by the fractional TPA cross section  $\delta_r^{ik}$  in the colormaps. Red spots represent the most dominant interstate coupling terms. In all cases, the diagonal term involving ES1,  $\delta_r^{11}$ , is the most dominant contributing term to the TPA cross section. In addition, cross coupling terms between ES1 and other states show minor contributions to the cross section, as represented with orange and blue spots for positive and negative values, respectively. The positive and negative contributions to the cross section are attributed to constructive and destructive interference among states, respectively. Specifically, destructive interference is observed if two transition matrix elements have different signs as a result of different symmetry. Despite the existence of multiple negative fractional cross sections

originating from destructive interference, the sum of all contributions is always positive as a single term dominates over the others. This result justifies the approximation of using one or two intermediate states in calculating cross section values.

The state-resolved analysis also shows how molecular structure and size affect the distribution of fractional cross sections for different states. A comparison between Figure 7A and B shows that the  $\delta_r^{11}$  value for 6T becomes less dominant compared to other fractional cross sections when the molecule is twisted. This is because the distorted structure results in a weaker transition matrix element between GS and ES1 which leads to a lower  $\delta_r^{11}$  value. For a larger molecular size, the distributions of fractional cross sections for 18T (Figure 7C and D) show that more states are involved in the total cross section as expected from the higher density of states. The choice of different final states (ES2 and ES3) yields a similar pattern of fractional TPA cross sections in which ES1 contributes dominantly and ES6 shows minor positive contributions, whereas ES7 and ES10 yield minor negative fractional cross sections. This hints that ES2 and ES3 play similar roles as the final state in determining the TPA cross section in terms of symmetry. However, the transition probability from ES1 is higher to ES3 than to ES2 and thereby results in a higher cross section. The transition density distributions for the first excitations (Figure S3) obviously form linearly distributed dipoles along the molecules. However, upper states with zero transition dipole moments are centrosymmetric.

Unlike classical TPA, the fractional ETPA cross sections provide significant information due to their strong oscillation with varying entanglement time. Specifically, different temporal behaviors are expected depending on the choice of intermediate states. In analogy to the fractional TPA cross section in eq 23, the fractional ETPA cross section is defined as follows:

$$\sigma_{\epsilon} \propto \langle S_{\epsilon}^{2} \rangle = \sum_{j,k} \langle \beta^{(j)} \beta^{(k)} \rangle [1 - \exp(-iT_{\epsilon} \Delta^{(j)} - T_{\epsilon} \kappa_{j}/2)]$$

$$\times [1 - \exp(-iT_{\epsilon} \Delta^{(k)} - T_{\epsilon} \kappa_{k}/2)] \propto \sum_{j,k} \sigma_{\epsilon}^{jk}$$
(24)

In Figure 8, total and fractional ETPA cross sections for 6T and 18T are plotted as a function of  $T_e$  for  $\omega=3.1$  eV and  $\kappa=0.0$  eV. A careful look at the peaks and dips of the total cross section (bold black curves) indicates that a single wave dominates the behavior of the total ETPA cross section, with minor interference with other small waves. As is the case with classical TPA,  $\sigma_e^{11}$  (blue bold curves) is the most dominant fractional cross section for both 6T and 18T. Therefore, the oscillation period of the total ETPA cross section can be approximated to that of  $\sigma_e^{11}$ . When the coupling states are identical  $(|j\rangle = |k\rangle$ ), the fractional ETPA cross section can be written as follows:

$$\sigma_e^{jj} \propto \langle \beta^{(j)2} \rangle [1 + e^{-T_{i}K_j} - 2e^{-T_{i}K_j/2} \cos(T_e \Delta_k^{(j)})]$$
 (25)

According to eq 25, the cross section oscillates with a period of  $2\pi/\Delta_{F}^{(j)}$ . As discussed in Figure 6, the ETPA cross sections oscillate with shorter periods for 6T than for 18T. The calculated periods with j = ES1 are 19 and 17 fs for planar and twisted 6T, respectively. (Figure 8A and B) However, longer periods of oscillation with a value of 30 fs are observed for 18T when either ES2 or ES3 is chosen as the final state. (Figure 8C and D) Although the oscillations in total cross sections are dominated by a single state, attenuation of the peak intensities is observed due to multiple minor contributions. Thus, we expect the peaks and dips in the ETPA cross section as a function of  $T_e$  to be less sharp as the size of the molecule increases. The dependence of the ETPA oscillations on the excited state line widths  $\kappa_i$  is even more dramatic. In Figure S4, ETPA cross sections are plotted as a function of  $T_e$  with  $\kappa_i$  = 0.1 eV. The dephasing in the excited states leads to a decrease in the coherence between the entangled photons and the electronic states. Therefore, oscillations in the ETPA cross section become featureless with increasing entanglement time. As the amount of coherence between the photonic and electronic states diminishes, the magnitude of the transition matrix elements dominates in determining the ETPA cross section, approaching the classical limit. Here we conclude that the increased molecular size and broader state line width can lead to decreased coherence in the ETPA process. In addition, any factors that increase the degrees of freedom of the molecule such as vibronic coupling, interactions with surrounding medium, and intermolecular interaction are likely to result in further decoherence. Experimentally, the dependence of the ETPA cross section on  $T_e$  is poorly studied due to technical limitations. Further experimental improvements with a better temporal resolution will offer detailed information

regarding the relationship between the ETPA cross sections and the electronic structure of a molecule.

## CONCLUSIONS

In summary, we developed a new theoretical method for calculating TPA and ETPA cross sections for relatively large organic chromophores and have used it to provide a quantitative interpretation of TPA/ETPA measurements. The second linear response TDDFT method was used to efficiently calculate the transition dipoles and excitation frequencies for the dominant excited states that correspond to absorption of the first or second photon. For both unentangled TPA and ETPA, the calculated cross sections were in good agreement with previously determined experimental values. A new feature in this work is that we use the radiative lifetime of the twophoton excited state to define the line width used in calculating the ETPA cross section. We justify this result by examining the interaction of an entangled photon pair with a three level system, showing that the two-photon radiative lifetime defines the entangled line shape as long as this lifetime is much longer than the intermediate state lifetime. The difference between the radiative lifetime of the entangled and unentangled states plays a major role in making the ETPA cross section many orders of magnitude larger than the TPA result. Finally we have examined the role of each intermediate state in the TPA and EPTA cross sections. This shows that various factors including molecular size, shape, excited state line width, and the choice of the excited state can affect oscillation patterns in the ETPA cross section. Such factors can be studied by resolving the ETPA cross section into two components: one related to the contribution of transition probabilities which scales with the TPA cross section, and one which scales with the two-photon radiative lifetime. Our results in this work show that the first term grows larger with increasing molecular size, but in general the second one shows a nonsystematic variation with molecular size. This conclusion indicates that in future work it will be important to search for rules governing the radiative lifetimes of two-photon excited states. In conclusion, our study successfully provides a pathway to interpret the interaction between entangled photons and relatively large molecules, which is of relevance to a number of chemical applications related to quantum light.

### ASSOCIATED CONTENT

#### Supporting Information

The Supporting Information is available free of charge at https://pubs.acs.org/doi/10.1021/jacs.0c02808.

Line shape for entangled two-photon emission (three state model and second order temporal correlation function are included), transition density plots, and ETPA cross section plots at  $\kappa_i = 0.1$  eV (PDF)

# AUTHOR INFORMATION

# **Corresponding Author**

George C. Schatz — Department of Chemistry, Northwestern University, Evanston, Illinois 60208, United States;
orcid.org/0000-0001-5837-4740; Email: g-schatz@northwestern.edu

#### **Authors**

- Gyeongwon Kang Department of Chemistry, Northwestern University, Evanston, Illinois 60208, United States;
  orcid.org/0000-0002-8219-2717
- Kobra Nasiri Avanaki Department of Chemistry, Northwestern University, Evanston, Illinois 60208, United States; Department of Chemistry and Chemical Biology, Harvard University, Cambridge, Massachusetts 02138, United States; oorcid.org/0000-0001-9975-7991
- Martín A. Mosquera Department of Chemistry, Northwestern University, Evanston, Illinois 60208, United States;
  ocid.org/0000-0003-2170-5651
- Ryan K. Burdick Department of Chemistry, University of Michigan, Ann Arbor, Michigan 48109, United States; orcid.org/0000-0002-3249-7993
- Juan P. Villabona-Monsalve Department of Chemistry, University of Michigan, Ann Arbor, Michigan 48109, United States; ⊚ orcid.org/0000-0002-0964-5855
- Theodore Goodson, III Department of Chemistry, University of Michigan, Ann Arbor, Michigan 48109, United States; orcid.org/0000-0003-2453-2290

Complete contact information is available at: https://pubs.acs.org/10.1021/jacs.0c02808

#### **Notes**

The authors declare no competing financial interest.

#### ACKNOWLEDGMENTS

G.K., M.M., T.G., and G.C.S. were supported by NSF Eager Grant CHE-1836392 (for two-photon research), and K.A. and G.C.S. were supported by NSF Grant CHE-1760537 (for entangled emission and absorption). This manuscript is dedicated to the memory of Richard P. Van Duyne, who recently passed away.

# **■** REFERENCES

- (1) Göppert-Mayer, M. Über elementarakte mit zwei quantensprüngen. Ann. Phys. 1931, 401, 273-294.
- (2) Schlawin, F.; Dorfman, K. E.; Mukamel, S. Entangled two-photon absorption spectroscopy. *Acc. Chem. Res.* **2018**, *51*, 2207–2214.
- (3) Maruo, S.; Nakamura, O.; Kawata, S. Three-dimensional microfabrication with two-photon-absorbed photopolymerization. *Opt. Lett.* **1997**, *22*, 132–134.
- (4) Ueno, K.; Juodkazis, S.; Shibuya, T.; Yokota, Y.; Mizeikis, V.; Sasaki, K.; Misawa, H. Nanoparticle plasmon-assisted two-photon polymerization induced by incoherent excitation source. *J. Am. Chem. Soc.* **2008**, *130*, 6928–6929.
- (5) Strickler, J. H.; Webb, W. W. Three-dimensional optical data storage in refractive media by two-photon point excitation. *Opt. Lett.* **1991**, *16*, 1780–1782.
- (6) Cumpston, B. H.; Ananthavel, S. P.; Barlow, S.; Dyer, D. L.; Ehrlich, J. E.; Erskine, L. L.; Heikal, A. A.; Kuebler, S. M.; Lee, I.-Y. S.; McCord-Maughon, D.; Qin, J.; Röckel, H.; Rumi, M.; Wu, X.-L.; Marder, S. R.; Perry, J. W. Two-photon polymerization initiators for three-dimensional optical data storage and microfabrication. *Nature* 1999, 398, 51.
- (7) Zhou, W.; Kuebler, S. M.; Braun, K. L.; Yu, T.; Cammack, J. K.; Ober, C. K.; Perry, J. W.; Marder, S. R. An efficient two-photon-generated photoacid applied to positive-tone 3D microfabrication. *Science* **2002**, *296*, 1106–1109.
- (8) Walla, P. J.; Linden, P. A.; Hsu, C.-P.; Scholes, G. D.; Fleming, G. R. Femtosecond dynamics of the forbidden carotenoid S1 state in light-harvesting complexes of purple bacteria observed after two-

- photon excitation. Proc. Natl. Acad. Sci. U. S. A. 2000, 97, 10808-10813.
- (9) Oar, M. A.; Dichtel, W. R.; Serin, J. M.; Fréchet, J. M.; Rogers, J. E.; Slagle, J. E.; Fleitz, P. A.; Tan, L.-S.; Ohulchanskyy, T. Y.; Prasad, P. N. Light-harvesting chromophores with metalated porphyrin cores for tuned photosensitization of singlet oxygen via two-photon excited FRET. Chem. Mater. 2006, 18, 3682–3692.
- (10) O'brien, J. L. Optical quantum computing. *Science* **2007**, *318*, 1567–1570.
- (11) Hadfield, R. H. Single-photon detectors for optical quantum information applications. *Nat. Photonics* **2009**, *3*, 696.
- (12) O'brien, J. L.; Furusawa, A.; Vučković, J. Photonic quantum technologies. *Nat. Photonics* **2009**, 3, 687.
- (13) Kocher, C. A.; Commins, E. D. Polarization correlation of photons emitted in an atomic cascade. *Phys. Rev. Lett.* **1967**, *18*, 575.
- (14) Benson, O.; Santori, C.; Pelton, M.; Yamamoto, Y. Regulated and entangled photons from a single quantum dot. *Phys. Rev. Lett.* **2000**, *84*, 2513.
- (15) Akopian, N.; Lindner, N.; Poem, E.; Berlatzky, Y.; Avron, J.; Gershoni, D.; Gerardot, B.; Petroff, P. Entangled photon pairs from semiconductor quantum dots. *Phys. Rev. Lett.* **2006**, *96*, 130501.
- (16) Salter, C.; Stevenson, R.; Farrer, I.; Nicoll, C.; Ritchie, D.; Shields, A. An entangled-light-emitting diode. *Nature* **2010**, *465*, 594.
- (17) Stevenson, R. M.; Young, R. J.; Atkinson, P.; Cooper, K.; Ritchie, D. A.; Shields, A. J. A semiconductor source of triggered entangled photon pairs. *Nature* **2006**, 439, 179.
- (18) Troiani, F.; Tejedor, C. Entangled photon pairs from a quantum-dot cascade decay: The effect of time reordering. *Phys. Rev. B: Condens. Matter Mater. Phys.* **2008**, 78, 155305.
- (19) Avanaki, K. N.; Schatz, G. C. Entangled photon resonance energy transfer in arbitrary media. *J. Phys. Chem. Lett.* **2019**, *10*, 3181–3188.
- (20) Saleh, B. E.; Jost, B. M.; Fei, H.-B.; Teich, M. C. Entangled-photon virtual-state spectroscopy. *Phys. Rev. Lett.* **1998**, *80*, 3483.
- (21) Lee, D.-I.; Goodson, T. Entangled photon absorption in an organic porphyrin dendrimer. *J. Phys. Chem. B* **2006**, *110*, 25582–25585.
- (22) Harpham, M. R.; Süzer, O.; Ma, C.-Q.; Bäuerle, P.; Goodson, T., III Thiophene dendrimers as entangled photon sensor materials. *J. Am. Chem. Soc.* **2009**, *131*, 973–979.
- (23) Guzman, A. R.; Harpham, M. R.; Süzer, O.; Haley, M. M.; Goodson, T. G., III Spatial control of entangled two-photon absorption with organic chromophores. *J. Am. Chem. Soc.* **2010**, 132, 7840–7841.
- (24) Upton, L.; Harpham, M.; Suzer, O.; Richter, M.; Mukamel, S.; Goodson, T., III Optically excited entangled states in organic molecules illuminate the dark. *J. Phys. Chem. Lett.* **2013**, *4*, 2046–2052.
- (25) Eshun, A.; Cai, Z.; Awies, M.; Yu, L.; Goodson, T., III Investigations of thienoacene molecules for classical and entangled two-photon absorption. *J. Phys. Chem. A* **2018**, *122*, 8167–8182.
- (26) Fei, H.-B.; Jost, B. M.; Popescu, S.; Saleh, B. E.; Teich, M. C. Entanglement-induced two-photon transparency. *Phys. Rev. Lett.* **1997**, 78, 1679.
- (27) Peřina, J.; Saleh, B. E.; Teich, M. C. Multiphoton absorption cross section and virtual-state spectroscopy for the entangled n-photon state. *Phys. Rev. A: At., Mol., Opt. Phys.* **1998**, *57*, 3972.
- (28) Burdick, R. K.; Varnavski, O.; Molina, A.; Upton, L.; Zimmerman, P.; Goodson, T., III Predicting and controlling entangled two-photon absorption in diatomic molecules. *J. Phys. Chem. A* **2018**, *122*, 8198–8212.
- (29) Roslyak, O.; Marx, C. A.; Mukamel, S. Nonlinear spectroscopy with entangled photons: Manipulating quantum pathways of matter. *Phys. Rev. A: At., Mol., Opt. Phys.* **2009**, *79*, 033832.
- (30) Schlawin, F.; Dorfman, K. E.; Fingerhut, B. P.; Mukamel, S. Manipulation of two-photon-induced fluorescence spectra of chromophore aggregates with entangled photons: A simulation study. *Phys. Rev. A: At., Mol., Opt. Phys.* **2012**, *86*, 023851.

- (31) Schlawin, F.; Mukamel, S. Two-photon spectroscopy of excitons with entangled photons. *J. Chem. Phys.* **2013**, *139*, 244110.
- (32) Jechow, A.; Seefeldt, M.; Kurzke, H.; Heuer, A.; Menzel, R. Enhanced two-photon excited fluorescence from imaging agents using true thermal light. *Nat. Photonics* **2013**, *7*, 973.
- (33) Dayan, B.; Pe'Er, A.; Friesem, A. A.; Silberberg, Y. Two photon absorption and coherent control with broadband down-converted light. *Phys. Rev. Lett.* **2004**, *93*, 023005.
- (34) Mosquera, M. A.; Chen, L. X.; Ratner, M. A.; Schatz, G. C. Sequential double excitations from linear-response time-dependent density functional theory. *J. Chem. Phys.* **2016**, *144*, 204105.
- (35) Mosquera, M. A.; Jackson, N. E.; Fauvell, T. J.; Kelley, M. S.; Chen, L. X.; Schatz, G. C.; Ratner, M. A. Exciton absorption spectra by linear response methods: application to conjugated polymers. *J. Am. Chem. Soc.* **2017**, *139*, 3728–3735.
- (36) Bebb, H. B.; Gold, A. Multiphoton ionization of hydrogen and rare-gas atoms. *Phys. Rev.* **1966**, *143*, 1.
- (37) Peticolas, W. L. Multiphoton spectroscopy. Annu. Rev. Phys. Chem. 1967, 18, 233–260.
- (38) Beerepoot, M. T.; Friese, D. H.; List, N. H.; Kongsted, J.; Ruud, K. Benchmarking two-photon absorption cross sections: performance of CC2 and CAM-B3LYP. *Phys. Chem. Chem. Phys.* **2015**, *17*, 19306—19314.
- (39) Albota, M.; Beljonne, D.; Brédas, J.-L.; Ehrlich, J. E.; Fu, J.-Y.; Heikal, A. A.; Hess, S. E.; Kogej, T.; Levin, M. D.; Marder, S. R.; McCord-Maughon, D.; Perry, R. H.; Joseph, W.; Rumi, M.; Subramaniam, G.; Webb, W. W.; Wu, X.-L.; Xu, C. Design of organic molecules with large two-photon absorption cross sections. *Science* 1998, 281, 1653–1656.
- (40) Beverina, L.; Fu, J.; Leclercq, A.; Zojer, E.; Pacher, P.; Barlow, S.; Van Stryland, E. W.; Hagan, D. J.; Brédas, J.-L.; Marder, S. R. Two-photon absorption at telecommunications wavelengths in a dipolar chromophore with a pyrrole auxiliary donor and thiazole auxiliary acceptor. *J. Am. Chem. Soc.* **2005**, *127*, 7282–7283.
- (41) Zheng, S.; Leclercq, A.; Fu, J.; Beverina, L.; Padilha, L. A.; Zojer, E.; Schmidt, K.; Barlow, S.; Luo, J.; Jiang, S.-H.; Jen, A. K.-Y.; Yi, Y.; Shuai, Z.; Van Stryland, E. W.; Hagan, D. J.; Brédas, J.-L.; Marder, S. R. Two-photon absorption in quadrupolar bis (acceptor)-terminated chromophores with electron-rich bis (heterocycle) vinylene bridges. *Chem. Mater.* 2007, 19, 432–442.
- (42) Masunov, A.; Tretiak, S. Prediction of two-photon absorption properties for organic chromophores using time-dependent density-functional theory. *J. Phys. Chem. B* **2004**, *108*, 899–907.
- (43) Monson, P.; McClain, W. Polarization dependence of the two-photon absorption of tumbling molecules with application to liquid 1-chloronaphthalene and benzene. *J. Chem. Phys.* **1970**, *53*, 29–37.
- (44) Scully, M.; Zubairy, M. S. Quantum Optics; Cambridge University Press: Cambridge, UK, 1997.
- (45) Muthukrishnan, A.; Agarwal, G. S.; Scully, M. O. Inducing disallowed two-atom transitions with temporally entangled photons. *Phys. Rev. Lett.* **2004**, *93*, 093002.
- (46) Kojima, J.; Nguyen, Q.-V. Entangled biphoton virtual-state spectroscopy of the  $A2\Sigma+-X2\Pi$  system of OH. Chem. Phys. Lett. **2004**, 396, 323–328.